Northern England Serpukhovian (early Namurian) farfield responses to southern hemisphere glaciation

M.H. STEPHENSON[1], L. ANGIOLINI[2], P. CÓZAR[3], F. JADOUL[2], M.J. LENG[4], D. MILLWARD[5], S. CHENERY[1]

[1]*British Geological Survey, Keyworth, Nottingham, NG12 5GG, United Kingdom*

[2]*Dipartimento di Scienze della Terra "A. Desio", Università degli Studi di Milano, Via Mangiagalli 34, Milano, 20133, Italy*

[3]*Instituto de Geología Económica CSIC-UCM; Facultad de Ciencias Geológicas; Departamento de Paleontología; C./ José Antonio Novais 228040-Madrid; Spain*

[4]*NERC Isotope Geosciences Laboratory, British Geological Survey, Keyworth, Nottingham, NG12 5GG, United Kingdom*

[5]*British Geological Survey, Murchison House, Edinburgh, United Kingdom*

Word count 7967

7 figs

1 table

67 references

RUNNING HEADER: NAMURIAN FARFIELD GLACIATION REPONSE

Abstract: During the Serpukhovian (early Namurian) icehouse conditions were initiated in the southern hemisphere; however nearfield evidence is inconsistent: glaciation appears to have started in limited areas of eastern Australia in the earliest Serpukhovian, followed by a long interglacial, whereas data from South America and Tibet suggest glaciation throughout the Serpukhovian. New farfield data from the Woodland, Throckley and Rowlands Gill boreholes in northern England allow this inconsistency to be addressed. $\delta^{18}O$ from well-preserved late Serpukhovian (late Pendleian to early Arnsbergian) Woodland brachiopods vary between –3.4 and –6.3‰, and $\delta^{13}C$ varies between –2.0 and +3.2‰, suggesting a $\delta^{18}O$ seawater (w) value of around –1.8‰ VSMOW, and therefore an absence of widespread ice-caps. The organic carbon $\delta^{13}C$ upward increasing trend in the Throckley Borehole (Serpukhovian to Bashkirian; c. –24 to c. –22‰), and the Rowlands Gill Borehole (Serpukhovian; c. –24 to c. –23‰) suggests large-scale burial of organic material, probably in burgeoning lycophyte-dominated coal forest, implying a fall in pCO_2. ρCO_2reduction appears not to have caused large-scale glaciation until the early Bashkirian, but a scenario of coalescing upland icecaps through the Serpukhovian with a background of decreasing ρCO_2, appears to be similar to the process that initiated Cenozoic Antarctic glaciation.

Keywords: Namurian, glaciation, isotopes, brachiopods, foraminifera

The mechanism and timing of the initiation of major glaciation in the Carboniferous are not well understood (Frank *et al*. 2008). Farfield carbonate fossils allow the examination of the carbon cycle through carbon isotope ratios ($\delta^{13}C$), while oxygen isotope ratios

43 ($\delta^{18}O$) serve as proxies for temperature and ice volume (Grossman *et al*. 2008). $\delta^{13}C$
44 values of terrestrial organic matter (plant fossils, cuticles, humic coals and bulk terrestrial
45 material) are related to large-scale carbon cycle changes such as burial of carbon in
46 decomposition-resistant lignin and reduction in atmospheric ρCO_2. However, the
47 interplay of these factors in individual periods of accelerated change requires careful
48 study. One such period is the Serpukhovian Stage (early Namurian; Pendleian –
49 Arnsbergian; Fig. 1) at which time glacial facies in South America, eastern Australia and
50 Tibet became established (see Isbell *et al*. 2003; González-Bonorino & Eyles 1995;
51 Fielding *et al*. 2008a). This period, the start of Glacial II of Isbell *et al*. (2003), is rather
52 poorly represented in terms of farfield oxygen and carbon isotopic data (Batt *et al*. 2007).

53 In eastern Australia, Glacial II begins with a short glacial period (termed C1; Fielding *et*
54 *al.* 2008a; Fig. 1) starting at 326.5 Ma (Menning *et al*. 2000) with duration about 1Ma.
55 This is recorded in only two locations, one of which is dated by SHRIMP U-Pb (Fielding
56 *et al.* 2008a; their fig 2). A period without evidence for eastern Australian glaciation
57 followed between 325 and 322 Ma, comprising the middle part of the Serpukhovian (late
58 Pendleian and early Arnsbergian; Gradstein *et al*. 2004). Isbell *et al*. (2003) considered
59 there to be evidence for glaciation in this period outside eastern Australia, in South
60 America and Tibet, based on correlations with the *Levipustula* Biozone in Australia (Fig.
61 1). A more widespread 'C2' glaciation is recognised in the late Serpukhovian (322.5 –
62 319.5 Ma, according to Fielding *et al*. 2008a), recorded in four separate locations in
63 Queensland and New South Wales.

64 The recent compilation of Frank *et al*. (2008) for brachiopods brought together the few
65 Serpukhovian data from the US midcontinent and Russian platform (Veizer *et al.* 1999

and Mii *et al.* 1999) and confirmed the wide range of $\delta^{18}O_{carb}$ and $\delta^{13}C_{carb}$ values (e.g. $\delta^{18}O_{carb}$ = –8.16 to –1.03‰ for the Donetsk Arnsbergian D5/1 Zone) for single horizons with corresponding low $\delta^{13}C_{carb}$. They thus noted a discrepancy between presumed onset of glacial activity in the early Serpukhovian and isotopic trends which suggest low ice volume until the early Bashkirian when brachiopod carbonate $\delta^{18}O$ increased (see also Buggisch *et al*. 2008). This discrepancy, the low sampling density and the wide range of values from single horizons indicate the need for new studies of accurately dated Serpukhovian sections with well preserved brachiopods.

The carbon isotope composition of terrestrial organic matter ($\delta^{13}C_{org}$) potentially has greater ability to track carbon cycle changes because of the ubiquitous nature of organic matter within sedimentary rocks. A detailed record of Serpukhovian $\delta^{13}C_{org}$ has yet to be presented and analysed in the context of isotopic, glacial or climate change. Strauss & Peters-Kottig (2003) and Peters-Kottig *et al*. (2006) measured $\delta^{13}C_{org}$ from terrestrial organic matter from plant fossils, cuticles, humic coals and bulk terrestrial material throughout the Late Palaeozoic. High values of terrestrial $\delta^{13}C_{org}$ (–21‰ to –22‰) between the early Mississippian and the Early Permian were attributed to the rise of large vascular land plants and associated burial of carbon in decomposition-resistant lignin. A long, low-gradient $\delta^{13}C_{org}$ increasing trend extends from the late Mississippian through the Pennsylvanian (Strauss & Peters-Kottig 2003, their fig. 3; Peters-Kottig *et al*. 2006, their fig. 1). A similar trend was noted through part of this period in the Throckley and Rowlands Gill boreholes in northern England by Stephenson *et al*. (2008).

Here new brachiopod $\delta^{18}O_{carb}$ and $\delta^{13}C_{carb}$ data from well-dated Serpukhovian horizons in the northern England borehole at Woodland are combined with Serpukhovian to

Bashkirian $\delta^{13}C_{org}$ data from nearby Throckley and Rowlands Gill boreholes, to track farfield isotopic changes in the context of known glacial activity in the southern hemisphere and particularly in eastern Australia.

Geological setting

The Namurian (Serpukhovian – early Bashkirian) rocks of northeast England consist of cycles of mixed clastic – carbonate facies, known locally as Yoredale cyclothems (Johnson 1984) or Yoredale cycles (Tucker *et al*. 2009). The Yoredale facies was deposited over an area of 10000 km^2 in northern England and southern Scotland and is particularly well developed on fault blocks such as the Alston Block, on which the Woodland (NZ 09096 27694) and Rowlands Gill (NZ 1664 5815) boreholes are situated (Fig. 2). The Throckley Borehole (NZ 14557 67617) is situated north of the Rowlands Gill borehole in the Northumberland Trough.

Yoredale cyclothems vary in thickness from around 5 to 50 m (Tucker *et al.* 2009) and consist of a lower carbonate part up to 30 m thick, overlain by a clastic section, sometimes capped by a coal seam or seatrock. The carbonate units vary from bioclastic lime mudstone to grainstone, but most are wackestone-packstone. These limestones are believed to have been deposited in the outer shoreface transition to the offshore environment in depths of 5 to 30 m. The clastic units are broadly deltaic, with shallowing-upward and coarsening-upward trends (mudstone to sandstone), occasionally incised into cycles below. Locally shoreline or marine sandbar facies also occur (Tucker *et al*. 2009).

In the Woodland Borehole, brachiopods were recovered in abundance from limestones (Faraday House Shell-Bed, Crag Limestone, and Rookhope Shell-Beds Limestone), and mudstones, particularly between the Crag Limestone and Rookhope Shell-Beds Limestone (Fig. 3). Samples for $\delta^{13}C_{org}$ were taken from mudstones and limestones in mainly transgressive parts of cyclothems in the Throckley and Rowlands Gill boreholes (Fig. 4).

Stratigraphically significant fossils occur in the sections and allow the brachiopod-bearing horizons and the horizons from which samples for $\delta^{13}C_{org}$ were taken to be precisely dated to the regional Carboniferous substages of Western Europe (Heckel & Clayton 2006) and in some cases to the standard global stages.

Age of the sections

Woodland Borehole brachiopod horizons

Rich foraminiferal assemblages were recorded from the lower part of the Woodland Borehole, from the Four Fathom and Great limestones (Figs. 1, 4, 5), including *Euxinita pendleiensis*, *Globivalvulina parva*, *Eostaffella pseudostruvei*, *E. angusta*, *E. acutiformis*, *E. postmosquensis*, *E. chomatifera*, *E. bashkirica, Monotaxinoides priscus*, *M. subplana, M. subconica*, *Endothyranella* and *Archaediscus* at "tenuis" stage. This assemblage is typical of the Serpukhovian, although some of the taxa may first occur in the latest Brigantian (Cózar & Somerville, 2004; Cózar *et al*., 2008). The Faraday House Shell-Bed contains few foraminiferans and most are not stratigraphically significant apart from rare *Archaediscus* at "tenuis" stage suggesting a Pendleian age. Amongst rare stratigraphically-significant macrofauna in the Woodland Borehole, Mills & Hull (1968)

also recorded the *Tylonautilus nodiferus* 'early mutation' of Stubblefield at 347.53 m (just below the Faraday House Shell-Bed), indicating the upper part of the Pendleian Stage (Figs. 1, 4). The Rookhope Shell-Beds Limestone contains rich foraminiferal assemblages, most of which persist from older Pendleian horizons; however, first occurrences include *Eostaffellina protvae*, *E. paraprotvae*, *Plectostaffella varvariensis*, *P. jahkensis* and *Eosigmoilina robertsoni*. *Eostaffellina protvae* and *E. paraprotvae* have only been recorded from the Protvinskian (Figs. 1, 4) in the Moscow Basin and lateral equivalents in the Urals Mountains and Donetsk, and are generally used as markers of the late Serpukhovian (e.g. Aisenverg *et al.* 1979, 1983; Einor 1996; Gibshman 2001; Vdovenko, 2001). *Plectostaffella* and *Eosigmoilina* are also considered late Serpukhovian markers in the Donetsk (Aisenverg *et al.* 1983; Vdovenko 2001) and Europe (Conil *et al.* 1991). In England and Scotland, *Eosigmoilina* is regarded as Arnsbergian by Fewtrell *et al.* (1981) and Riley (1992). The Grindstone Limestone (Fig. 4) contains the first occurrence of *Seminovella*, considered by Conil et al. (1980, 1991) as a Chokierian marker, but in Russia commonly described from the Zapaltubinsky horizon (late Arnsbergian). The Whitehouse Limestone contains *Plectostaffella bogdanovskensis*, typically recorded from the base of the Bashkirian of the Urals Mountains (Reitlinger in Einor *et al.* 1979).

The Woodland borehole was also studied for palynology by Neves (1968). The section between the Crag Limestone and Lower Fell Top Limestone (Fig. 4) contains *Bellispores nitidus*, *Crassispora kosankei*, *Grandispora spinosa*, *Remysporites magnificus, Tripartites trilinguis* and *T. vetustus*. According to Owens *et al*. (2004) *B. nitidus*, *G. spinosa*, *Remysporites magnificus* and *T. vetustus* range into the upper Arnsbergian

within the TK Biozone but not into the SV Biozone. This section also lacks *Rotaspora fracta*, *Verrucosisporites morulatus*, *Raistrickia nigra* and *Reticulatisporites carnosus* which disappear at the top of the preceding Vm Biozone. The distribution of taxa thus suggests that the section between the Crag Limestone and Lower Fell Top Limestone is Arnsbergian but not latest Arnsbergian in age (Owens *et al.* 2004), in broad agreement with the age suggested by foraminifera.

Sample horizons for $\delta^{13}C_{org}$ in Throckley and Rowlands Gill boreholes

Riley (1992) recorded a diverse foraminiferal fauna from the Lower Fell Top Limestone of the Rowlands Gill borehole, including *Eosigmoilina robertsoni* which he considered to be Arnsbergian. Similarly Riley considered the Upper Fell Top Limestone (Fig. 4) to be Arnsbergian in age. The lowest studied part of the Throckley Borehole between 358.33 and 243.23 m was assigned by Stephenson *et al.* (2008) to the latest Brigantian to Pendleian palynological *capistratus – nitidus* (CN) Biozone of Owens *et al*. (2004), though the top of the biozone was poorly defined because the base of the succeeding Biozone, the *trigallerus – knoxi* (TK) Biozone, cannot be positioned precisely. However ages from the Woodland Borehole can be adopted since the major limestones (e.g. the Whitehouse and Upper Fell Top limestones) can be correlated with confidence between the two boreholes.

Perhaps the most distinct palynostratigraphical level in the Throckley Borehole is marked by the late Alportian first appearance of common *Crassispora kosankei* at 126.5 m (KV Biozone, see Owens *et al.* 2004). The first occurrence of *Lycospora subtriquetra*, slightly lower, at 136 m, suggests that the *subtriquetra – ornatus* (SO) Biozone may extend from 136 to 126.5 m (late Arnsbergian to early Alportian; Owens *et al*. 2004).

Age conclusion

Dating shows that the age of the brachiopod section studied for $\delta^{13}C_{carb}$ and $\delta^{18}O_{carb}$ between the shales beneath the Crag Limestone and the Rookhope Shell-Beds Limestone is late Pendleian to early Arnsbergian (Protvinskian), and therefore would fall within the interglacial period between C1 and C2 of Fielding *et al.* (2008a; Fig 1).

The range of ages of the $\delta^{13}C_{org}$ horizons in the Throckley Borehole is from the late Brigantian - Pendleian CN Biozone to the late Alportian-early Marsdenian KV Biozone, while the range in age of the $\delta^{13}C_{org}$ horizons in the Rowlands Gill Borehole by correlation with the Throckley section is late Brigantian - Pendleian to approximately Arnsbergian. Thus, the $\delta^{13}C_{org}$ record in the Throckley Borehole encompasses much of the Serpukhovian and into the Bashkirian, while that in Rowlands Gill Borehole covers the lower and middle parts of the Serpukhovian (Fig. 1).

Materials and methods

The Woodland Borehole brachiopod specimens were rigorously screened by ultrastructural, cathodoluminescence and trace element geochemical analysis. Forty specimens were first selected for ultrastructural and cathodoluminescence analysis. Of these 36 underwent subsequent isotope analyses, and 19 also provided enough carbonate for additional trace element geochemical analysis (Table 1).

The selected brachiopods are *Antiquatonia hindi, A. costata*, *Skelidorygma* sp., *Anthracospirifer* sp., *Angiospirifer* sp., *A. trigonalis*, and *Merospirifer* sp. *Antiquatonia hindi* and *A. costata* are concavo-convex semi-infaunal productids which are found in mudstone and shale. *Skelidorygma* sp., *Anthracospirifer* sp., *Angiospirifer* sp., *A.*

200 *trigonalis*, and *Merospirifer* sp. are pediculate spiriferids which usually occur in
201 limestone. Semi-infaunal productids supported themselves with spines in soft substrates
202 in low energy environments generally on offshore platforms, at depth below the fair-
203 weather wave base (Brunton 1972, 1984, 1987). Pediculate taxa, particularly those with
204 large pedicle openings, indicate attachment to hard substrates in relatively high energy
205 environments, where the settling strategies require firm attachment to the substrate
206 (Brunton, 1987). They suggest firm substrates, higher energy, and depth around the fair-
207 weather wave base. The Woodland brachiopods thus comprise a mixture of shallow and
208 deeper water taxa, from a range of palaeoenvironmental conditions in different parts of
209 typical Yoredale cycles (Fig. 3).

210 The specimens were embedded in resin, cut along longitudinal and transverse sections,
211 then etched with 5% HCl for 20 s and metallic-coated before being investigated using
212 SEM to check the preservation of their shell fabric. In addition thin sections were made to
213 allow cathodoluminescence microscopy of the same sections.

214 Cathodoluminescence (CL) was performed using a cold cathode luminoscope (Nuclide
215 ELM2) operating at 10KV voltage with a current beam of 5-7 MA. This is a screening
216 technique widely used to assess preservation of brachiopod shells (Popp *et al.* 1986;
217 Grossman *et al.* 1993), as they commonly show no luminescence in absence of significant
218 geochemical alteration. However, its reliability to distinguish altered from unaltered
219 shells has been questioned (Korte *et al*. 2005, England *et al.* 2006). To overcome one of
220 the drawbacks of conventional optical CL (i.e. the fact that beam current conditions vary
221 in the different studies) we analysed all the thin sections of the brachiopod shells with the
222 same instrument operating under the same beam conditions.

223 The brachiopods were sampled for geochemical and isotope analysis by drilling 6-8
224 milligrams along the longitudinal section of each shell using a diamond drill bit. Only the
225 diagenetically-unaltered inner part of the thick secondary and tertiary shell layer of both
226 the ventral and dorsal valves was sampled for geochemical and isotope analyses (Table
227 1). Features such as the muscle attachment areas, articulation points, interareas and
228 lophophore support were avoided, although Parkinson *et al*. (2005) showed there is a
229 minimal risk when sampling specialised shell fragments.

230 Subsamples for geochemical analysis were dissolved in ultra-pure acetic acid. The acetic
231 acid leached fraction reserved for geochemistry (see below) was evaporated to dryness
232 and the residue taken up in 1% nitric acid. Geochemical data were obtained by
233 Inductively Coupled Plasma Atomic Emission Spectroscopy (ICP-AES) on a Fison/ARL
234 3580 simultaneous/sequential spectrometer with Gilson auto sampler.

235 Approximately 30-100 microgrammes of carbonate were used for isotope analysis using a
236 GV IsoPrime mass spectrometer plus Multiprep device. Isotope values ($\delta^{13}C$, $\delta^{18}O$) are
237 reported as per mille (‰) deviations of the isotopic ratios ($^{13}C/^{12}C$, $^{18}O/^{16}O$) calculated to
238 the VPDB scale using a within-run laboratory standard calibrated against NBS standards.
239 Analytical reproducibility of the standard calcite (KCM) is < 0.1‰ for $\delta^{13}C$ and $\delta^{18}O$.

240 All samples for organic carbon isotope analysis were treated to remove any migrated
241 hydrocarbons since these affect $\delta^{13}C_{org}$ bulk values, particularly if they are markedly
242 different in geochemical origin from the *in situ* material analysed (Stephenson *et al*.
243 2005). The hydrocarbons were removed by using a soxhlet apparatus on crushed samples
244 (Stephenson *et al*. 2005). In order to determine the $\delta^{13}C$ values of different fractions of
245 organic material, separate analyses were done on hydrocarbon-free rock samples and on

246 microscopic fossil wood fragments from the same rock samples. To obtain microscopic
247 fossil wood fragments, each sample was acid macerated in hydrofluoric acid, and the
248 organic residue rinsed and sieved into two different size fractions. The fraction 500-1000
249 µm size was exclusively of terrestrial vascular plant origin, dominated by dark brown or
250 black structured woody phytoclasts, and this was analysed to determine $\delta^{13}C$ of wood
251 fragments. %C was measured using a Carlo Erba 1500 elemental analyser, calibrated
252 against an Acetanilide standard in order to estimate the amount of material for isotope
253 analysis. Replicate analysis of well-mixed samples indicated a precision of $\pm$ <0.1%.
254 $^{13}C/^{12}C$ analyses were performed also using the Carlo Erba 1500 on-line to a VG
255 TripleTrap (plus secondary cryogenic trap in the mass spectrometer for these very low
256 carbon content samples) and Optima dual-inlet mass spectrometer, with $\delta^{13}C$ values
257 calculated to the VPDB scale using a within-run laboratory standard (BROC1) calibrated
258 against NBS-18 and NBS-19. Replicate analysis of well-mixed samples indicated a
259 precision of $\pm$ <0.1‰ (1 SD).

260

261 Results and discussion

262 *Shell structure*

263 All the brachiopod sections were analysed under SEM (see the ultrastructure summary in
264 Table 1). Most of the valves have a well-preserved shell succession consisting of a
265 secondary layer of fibres or laminae and a prismatic tertiary layer.

266 The secondary layer of the spiriferids (*Anthracospirifer* sp., *Angiospirifer* sp.,
267 *Angiospirifer trigonalis*) consists of long fibres with a keel and saddle profile in cross

section (Fig. 6 a-c). Internally, the secondary layer makes transition to a very thick prismatic tertiary layer by lateral spreading of the terminal face of each fibre and then by vertical accretion to form discrete prisms; they show interlocking boundaries normal to the surface of accretion and strong growth banding (Fig. 6 d-j). Some specimens show evidence of diagenetic alteration under SEM, the fibres of the secondary layer being recrystallized and amalgamated corresponding to type-3 (Fig. 6 k) and type-6 (Figs. l, 6) altered ultrastructures of Samtleben *et al.* (2001). However, generally the tertiary layer still shows growth banding and no sign of diagenetic alteration.

Few productid shells are well-preserved, with a laminar secondary layer of lath-like laminae alternating with a prismatic layer (BU6768 *Antiquatonia hindi*) (Fig. 6 m-n). Most productids show altered amalgamated laminae corresponding to type-9 ultrastructure (*Antiquatonia costata*; Fig. 6 o) of Samtleben *et al.* (2001).

Cathodoluminescence

The second and tertiary layers of all the analysed spiriferids were non-luminescent (NL) under CL, in agreement with their preserved ultrastructure and TE. Non-luminescent spiriferid shells are typically dull black in colour under CL, and they contrast with the orange luminescence of the bulk rock, which records several diagenetic events. Two specimens (BU8285, BU8292; Fig. 7) show luminescent dog-tooth cement encrusting their inner shell surface; in the associated bulk rock several brachiopod shells are encrusted by these cements on both sides (thin isopachous layer) suggesting shallow burial cementation or an early dissolution around bioclasts before cementation.

289 Productids are either NL or may show a slight luminescence parallel to the lath-like
290 laminae which form their secondary layer. The sources of cathodoluminescence in
291 biogenic carbonate are Mn^{++} and Fe^{++}, which tend to be more concentrated in those shells
292 which have an increased amount of intercrystalline organic material in the original *in vivo*
293 laminar fabric (Barbin *et al.* 1991; Griesshaber *et al.* 2007). The laminar fabric of
294 productids has a higher organic content (proteinaceous membranes) than the fibrous and
295 prismatic layers of spiriferids and tends to show a greater luminescence (Angiolini *et al.*
296 2008, 2009).

297

298 *Trace elements*

299 Well-preserved modern brachiopods from a variety of depositional environments display
300 Sr contents of 450-1930 ppm (µm/g), Mn from 1-199 ppm (µm/g), and Fe contents
301 generally <140 ppm (µm/g), although much higher values have also been reported (Brand
302 *et al.* 2003). Similar trace-element concentrations have been reported for Carboniferous
303 and Permian brachiopods, although Sr contents as high as 3400 ppm and Mn of 250 ppm
304 have also been measured in NL brachiopod shells (Popp *et al*. 1986). Korte et al. (2003)
305 adopted the criteria of <250 ppm Mn and >400 ppm Sr for samples to be classified as
306 well-preserved. Bruckschen *et al*. (1999) accepted a more conservative cut-off limit of
307 200 ppm for Mn, which they considered to be a more reliable indicator of diagenetic
308 alteration than Sr content. Van Geldern *et al*. (2006) classified shells with <100 ppm Mn
309 and >500 ppm Sr as well preserved.

310 Joachimski *et al*. (2005) showed that Silurian (1211-1830 ppm) and Devonian (758-1467
311 ppm) brachiopods have higher Sr concentration than those of the Late Carboniferous and
312 Early Permian. High Sr concentration in biological calcite before the Late Carboniferous

313 was related by Steuber & Veizer (2003) to the Ordovician-Mississippian calcite episode,
314 when strontium-rich biogenic calcite was formed from high Sr/Ca oceanic waters.

315 Woodland brachiopods were analyzed for TE where possible, but in some cases too little
316 carbonate was available after isotope analysis (Table 1). The brachiopods have Mn
317 contents <210 ppm (and 80% have Mn < 100 ppm) and Sr contents >500 ppm, which
318 indicates good preservation, based on most criteria described above. The analyses of the
319 bulk rock (Table 1) associated with two brachiopod specimens show much higher (>
320 2000 ppm) Mn contents. Fe is more variable in the brachiopods (106 - 4072 ppm), but
321 70% of the specimens have Fe < 1500 ppm; the higher values are suggested to result from
322 surface coatings of oxyhydroxides and come from brachiopods that were enclosed by
323 dark mudstone that probably contains pyrite. We do not consider variable Fe to be an
324 indicator of preservation, due to its insolubility under oxic conditions (Popp *et al*. 1986;
325 McArthur *et al*. 2000).

326 *Brachiopod isotope composition*

327 Brachiopods are central to carbon and oxygen isotope study because their shells are
328 considered to be usually well preserved, thus containing an ocean water composition
329 from the time of formation (Parkinson & Cusack in Williams *et al.* 2007; Grossman *et al*.
330 2008), and because rhynchonelliform brachiopod shells have a dense microstructure and
331 generally low Mg chemistry that make them resistant to diagenesis (Compston 1960;
332 Popp *et al.* 1986). In Carboniferous farfield studies, brachiopod specimens from the U.S.
333 Midcontinent and Russian Platform have mainly been used up to now, because of their
334 good preservation and wide geographic and temporal distribution. Samples from the U.S.
335 Midcontinent come from Texas, Oklahoma, Arkansas, Kansas, Nebraska, Iowa, Missouri,

Illinois, Idaho and Indiana (Grossman *et al.* 1991, 1993, 2008; Mii *et al*. 1999; Batt *et al.* 2007). Russian Platform samples are from the Moscow Basin and the Ural Mountains (Bruckschen *et al*. 1999, 2001; Mii *et al.* 2001; Grossman *et al.* 2002; Korte *et al.* 2005). In most cases these were broad surveys using a large number of analyses to indicate trends. In some cases, specimens were not identified other than as brachiopods, with many being small fragments, thus effects of generic or specific variation cannot be ruled out.

In the US Midcontinent and Russia, the later (Bashkirian) part of Glacial II of Isbell *et al.* (2003) is well represented by samples. High $\delta^{18}O$ and $\delta^{13}C$ values (~–1 to –2‰ and +4 to 5‰ respectively) are consistent with glaciation. However, the early part (Serpukhovian) is poorly represented. In the Moscow Basin there is a hiatus in the late Serpukhovian, and in the early Serpukhovian in the Donetsk Basin from where most Russian samples come (Bruckschen *et al.* 1999), there are very few sample points. Late Serpukhovian samples from the Askyn section in the Urals Mountains yield $\delta^{18}O$ values averaging −4.8‰. Bruckschen *et al.* (2001) suspected that these Serpukhovian samples might be influenced by freshwater influx during deposition, and Grossman *et al.* (2008) suspected diagenetic influence. There are similarly few horizons for sampling in the early Serpukhovian in the US Midcontinent (Grossman *et al.* 2008); Bishop *et al.* (2009) recorded brachiopod $\delta^{18}O$ values of approximately −3‰ in two horizons in the lowermost Indian Springs Formation. Middle and late Serpukhovian values average around −5‰ (Batt *et al.* 2007) and latest Serpukhovian $\delta^{18}O$ values are ~ –3‰ (Grossman *et al.* 2008; Brand & Brenckle 2001).

$\delta^{18}O$ values from pristine Woodland Borehole brachiopods vary between –3.4 and –6.3‰, whereas $\delta^{13}C$ vary between –2.0 and +3.2‰. The carbon isotope data lie within the range that is generally thought to represent Carboniferous seawater values (Grossman *et al.* 2008). The brachiopods comprise a mixture of shallow and deeper-water taxa, ranging in depth from below fair-weather wave base to a few metres and thus are unlikely to introduce bias due to temperature difference causing differences in $\delta^{18}O_{carb}$ (see Immenhauser *et al.*, 2003). Rhynchonelliform brachiopods are also known for low tolerance of variable salinity. Thus, it is likely that the Woodland brachiopods are representative of unrestricted ocean conditions.

The low $\delta^{18}O$ values from pristine Woodland Borehole brachiopods are very close to those recorded in the Late Devonian by Van Geldern *et al.* (2006), who showed a long term $\delta^{18}O$ decreasing trend, from a value of +2.8‰ in the Early Devonian to values between –4.3 and –6.1‰ in the latest Givetian and Late Devonian. Van Geldern *et al.* (2006) interpreted this secular decrease in $\delta^{18}O$ as due to a combination of climate warming and a moderate decrease in $\delta^{18}O$ of seawater (down to –2.4‰ V-SMOW).

Using the expression of Leng & Marshall (2004), from the equation of Kim & O'Neil (1997):

$$t = 13.8 - 4.58(c - w) + 0.08(c - w)^2$$

it is possible to obtain a maximum value for the $\delta^{18}O$ seawater (w) in the Serpukhovian, assuming a palaeo-seawater temperature (t) and using the Woodland brachiopod calcite average value (c). Assuming a seawater temperature (t) of 29°C (i.e. the modern tropical sea-surface temperature; Cahyarini *et al.* 2008) for the tropical setting of the Woodland Borehole brachiopods and using the average value obtained for the brachiopod calcite (c=

–5.0‰), the $\delta^{18}O$ seawater (w) would have been approximately –1.8‰ VSMOW. This value is consistent with the small range in $\delta^{18}O$ through the Palaeozoic indicated by the 'clumped isotope' palaeothermometer (see Came *et al.*, 2007; $\delta^{18}O$ values of −1.2±0.5‰VSMOWfor the Early Silurian and −1.6±0.1‰ VSMOW for the Middle Pennsylvanian).

One of the requirements for negative $\delta^{18}O$ seawater values is the absence of widespread ice-caps. Also, according to Van Geldern *et al.* (2006), continental weathering is an important sink for ^{18}O and may lower $\delta^{18}O$ seawater because the products of continental silicate weathering (clay minerals and other H_2O-bearing minerals) are enriched in ^{18}O, though this is considered a minor effect. Dilution by meteoric water may also lower $\delta^{18}O$ seawater (Van Geldern *et al.* 2006), but the presence of brachiopods in the Woodland section which are intolerant of low salinity, indicate that this was not a factor. Therefore the low $\delta^{18}O$ seawater suggested by Woodland Borehole brachiopods is most likely the result of the absence of widespread ice-caps during the late Pendleian to early Arnsbergian, in the interglacial interval between C1 and C2 (Fielding *et al.* 2008a).

Organic carbon isotopes

A long term statistically significant trend in the Throckley and Rowlands Gill boreholes, is increasing $\delta^{13}C_{org}$ (c. –24‰ to c. –22‰ in Throckley Borehole; Fig. 4; for details see Stephenson *et al.* 2008). In the Throckley Borehole the trend extends from within the Pendleian to the Chokierian (Fig. 1). This increasing trend is also mirrored in the lower parts of the boreholes by $\delta^{13}C$ from organic carbon separated from limestone (Fig. 4). The

403 trend was considered by Stephenson *et al.* (2008) to record global variation because (1) it
404 occurs in both boreholes; (2) the data come from a random collection of mainly wood
405 fragments; (3) wood fragments alone show the same trend (Fig 4); and (4) marine and
406 terrestrial $\delta^{13}C_{org}$ show the same trends (for detailed discussion see Stephenson *et al.*
407 2008). Stephenson et al. (2008) did not attempt to explain the pattern of $\delta^{13}C_{org}$; however
408 this is now possible in the context of recent information.

409 Wetland lycophyte-dominated palaeotropical forests ('coal forests') became widespread
410 in the Serpukhovian in central Asia and spread over the European Variscan foreland and
411 intramontane basins through the Serpukhovian, Bashkirian and Moscovian, declining in
412 the Kasimovian (Cleal & Thomas 2005). Lycophyte-dominated forests were an extremely
413 efficient carbon sink because of their high growth rates and because of low rates of
414 decomposition of vegetation litter due to low-pH substrates and low fungal activity,
415 burying 108 to 390 tonnes of carbon per hectare per annum. At their maximum
416 development in the late Moscovian, the lycophyte forest had a global area of 2395×10^3
417 km^2 which sequestered 93×10^9 tonnes of carbon per annum (Cleal & Thomas 2005).
418 During photosynthesis, ^{12}C is taken up preferentially to ^{13}C such that organic matter
419 derived from organisms is about 20‰ lower in ^{13}C than the carbon in atmospheric CO_2 or
420 dissolved inorganic carbon in seawater (Berner 2003). The process of burial of organic
421 material in rock therefore causes an increase in atmospheric $\delta^{13}C$ which is transferred to
422 plant tissue. This is the likely cause of the increase in $\delta^{13}C_{org}$ in the Throckley and
423 Rowlands Gill boreholes, and it would also suggest a steady decrease in pCO_2 which is
424 also indicated by coarse modelling through the whole of the Carboniferous – Permian
425 (Berner 2003) and by coarse sampling in the late Palaeozoic (Peters-Kottig *et al*. 2006).

426 Woodland Borehole carbonate $\delta^{13}C_{carb}$ (Fig. 4) does not occur over a long enough
427 stratigraphic range to discern a trend, but other studies of whole rock carbonate (e.g.
428 Buggisch *et al.* 2007) and brachiopod calcite (compilation by Frank *et al.* 2008) through
429 the late Serpukhovian into the Bashkirian show increasing trends interpreted as due to
430 carbon burial in terrestrial or marine environments.

431 Conclusions

432 Stable isotope composition of brachiopod carbonate in the Woodland Borehole indicates
433 seawater isotope composition during the middle part of the Serpukhovian that in turn
434 suggests ice-free conditions. This corresponds to the period between C1 and C2 of
435 Fielding *et al.* (2008a) and indicates that glaciation cannot have been widespread for a
436 substantial part of the Serpukhovian. $\delta^{13}C_{org}$ data from the nearby Throckley and
437 Rowlands Gill boreholes indicate a steady fall in pCO_2 throughout the Serpukhovian and
438 into the Bashkirian which is consistent with carbonate $\delta^{13}C$ trends as well as with the
439 worldwide rise of lycophyte-dominated coal forest.

440 Frank *et al.* (2008) commented on the discrepancy between low brachiopod $\delta^{18}O$ and
441 distribution of glacial facies in the Serpukhovian as suggested by Isbell *et al*. (2003), and
442 on the absence of a clear isotopic signature related to the onset of Glacial II. Thus they
443 suggested that Serpukhovian glaciation was geographically limited and that falling ρCO_2
444 and other factors may have lowered temperatures sufficiently by the Bashkirian to allow
445 the growth of continental glaciation which produced a consistent $\delta^{18}O$ response. Evidence
446 from rigorously-screened well dated brachiopods in the Woodland Borehole, and from

447 dated $\delta^{13}C_{org}$ horizons in Throckley and Rowlands Gill boreholes show this interpretation
448 to be largely correct and shows the value of targeted studies of farfield sections.

449 It is interesting to compare the onset of Cenozoic Antarctic glaciation with this process.
450 At about 34 Ma (earliest Oligocene), causes of cooling included ocean heat transport
451 changes due to palaeogeographic changes, but declining ρCO_2 was the dominant cause of
452 cooling and glaciation (Deconto & Pollard 2003). Early Cenozoic ρCO_2 was 2 to 5 times
453 greater than present day levels, declining to reach modern levels in the early Neogene
454 (Pearson & Palmer 2000). Deconto & Pollard (2003) showed that as ρCO_2 declined
455 causing a reverse greenhouse effect, the East Antarctic Ice Sheet enlarged from small
456 isolated ice caps into permanent ice caps. At ρCO_2 levels of 3x and 2x present levels,
457 height mass balance feedbacks were initiated during orbital periods producing cold
458 austral summers, in turn producing much larger terrestrial ice sheets. According to
459 Deconto & Pollard (2003), within a single 40ka obliquity cycle, ice sheets reached sea
460 level around most of the continental margin of Antarctica. Although the cause of ρCO_2
461 decrease was different in the Cenozoic (likely reductions in outgassing from volcanoes)
462 because Cenozoic forests were not as efficient carbon sinks as lycophyte-dominated coal
463 forest, it is likely that a similar mechanism of increased glacial nucleation with a
464 background of decreasing ρCO_2 caused the Bashkirian onset of large-scale glaciation.

465 In summary, the Woodland, Throckley and Rowlands Gill sections show that at least one
466 substantial period between the C1 and C2 glaciations in eastern Australia cannot have
467 experienced cold temperature or large-scale glaciation. This casts doubt on the
468 proposition that Glacial II of Isbell *et al*. (2003) began substantially in the Serpukhovian
469 and supports the model developed from compilations by Fielding *et al.* (2008b) that the

Serpukhovian saw only isolated ice centres, whereas the start of the Bashkirian saw a much greater broadening of ice. The sections also show that a steady fall in ρCO_2 occurred throughout the Serpukhovian and into the Bashkirian. These events were likely related to a slow increase in glaciation from small nuclei in upland areas in the early Serpukhovian to continental glaciation in the Bashkirian.

Joanne Green and Chris Kendrick are thanked for the stable isotope analysis. M. H. Stephenson, M. J. Leng, S. Chenery and D. Millward publish with permission of the Executive Director of the British Geological Survey (NERC). M. Howe, BGS Collections Manager, kindly allowed access to brachiopods from the Woodland Borehole. P. Brand selected suitable brachiopod material. P. Cózar acknowledges financial support from Projects CGL2006-03085 and CGL2009-10340 (Ministerio de Ciencia e Innovación), Spain. C. Malinverno and A. Rizzi are also thanked for technical assistance.

References

Aisenverg, D. E., Brazhnikova, N. E., Vassilyuk, N. P., Reitlinger, E. A., Fomina, E. V., Einor, O. L. 1979. The Serpukhovian stage of the Lower Carboniferous of the USSR. *In*: Wagner, R.H., Higgins, A.C., Meyen, S.V. (eds.), *The Carboniferous of the USSR*. Yorkshire Geological Society, Occasional Publication 4. pp. 43–59.

490 Aizenverg, D. E., Astakhova, T. V., Berchenko, O. I., Brazhnikova, N. E., Vdovenko, M.
491 V., Dunaeva, N. N., Zernetskaya, N. V., Poletaev, V. I., Sergeeva, M. T. 1983.
492 Verkhneserpukhovskii podyarus Donetskogo basseina (*Late Serpukhovian substage in*
493 *the Donets Basin*). Akademiya Nauk Ukrainskoi SSR, Institut Geologicheskii Nauk. pp
494 1–164. (in Russian).

495 Angiolini, L., Darbyshire, D. P. F, Stephenson, M. H., Leng, M. J., Brewer, T. S., Berra,
496 F. & Jadoul, F. 2008. Lower Permian brachiopods from Oman: their potential as climatic
497 proxies. *Earth and Environmental Science Transactions of the Royal Society of*
498 *Edinburgh*, **98**, 1–18.

499 Angiolini, L., Jadoul, F., Leng, M. J., Stephenson, M. H., Rushton, J., Chenery, S., &
500 Crippa, G. 2009. How cold were the Early Permian glacial tropics? Testing sea surface
501 temperature using the oxygen isotope composition of brachiopod shells. *Journal of the*
502 *Geological Society of London*, **166**, 933-945.

503 Barbin, V., Ramseyer, K., Debenay, J. P., Schein, E., Roux, M. & Decrouex, D. 1991.
504 Cathodoluminescence of recent biogenic carbonates: an environmental and ontogenetic
505 fingerprint. *Geological Magazine* **128**, 19-26.

506 Batt, L. S., Montanez, I. P., Isaacson, P., Pope, M. C., Butts, S. H. & Abplanalp, J. 2007.
507 Multi-carbonate component reconstruction of Mid – Carboniferous (Chesterian) seawater
508 $\delta^{13}C$. *Palaeogeography, Palaeoclimatology, Palaeoecology*, **256**, 298-318.

509 Berner, R.A. 2003. The long-term carbon cycle, fossil fuels and atmospheric
510 composition. *Nature*, **426**, 323-326.

511 Bishop, J. W., Montanez, I. P., Gulbranson, E. L. & Brenckle, P. L. 2009. The onset of
512 mid-Carboniferous glacio-eustasy: sedimentologic and diagenetic constraints, Arrow
513 Canyon, Nevada. *Palaeogeography, Palaeoclimatology, Palaeoecology*, **276**, 217-243.

514 Brand, U. & Brenckle, P. 2001. Chemostratigraphy of the mid-Carboniferous boundary
515 global stratotype section and point (GSSP), Bird Spring Formation, Arrow Canyon,
516 Nevada, USA. *Palaeogeography, Palaeoclimatology, Palaeoecology*, **165**, 321-347.

517 Brand, U., Logan, A., Hiller, N. & Richardson, J. 2003. Geochemistry of modern
518 brachiopods: applications and implications for oceanography and paleoceanography.
519 *Chemical Geology,* **198**, 305-334.

520 Bruckshen, P., Oesmann, S. & Veizer, J. 1999. Isotope stratigraphy of the European
521 Carboniferous. Proxy signals for ocean chemistry, climate and tectonics. *Chemical*
522 *Geology*, **161**, 127-163.

523 Bruckschen, P., Veizer, J., Schwark, L., & Leythaeuser, D. 2001. Isotope stratigraphy for
524 the transition from the late Paleozoic greenhouse in the Permo-Carboniferous icehouse –
525 new results. *Terra Nostra*, **7-112001/4**.

526 Brunton, C. H. C. 1972. The shell structure of chonetacean brachiopods and their
527 ancestors. *Bulletin of British Museum (Natural History), Geology,* **21**, 1-26.

528 Brunton, C. H. C.1984. Growth and shell shape in productacean brachiopods. *Bulletin of*
529 *British Museum (Natural History), Geology,* **38**, 273-281.

530 Brunton, C. H. C. 1987. The palaeoecology of brachiopods and other faunas, of Lower
531 Carboniferous (Asbian) limestones in West Fermanagh. *Irish Journal of Earth Sciences*,
532 **8**, 97-112.

533 Buggisch, W., Joachimski, M. M. Sevastopulo, G., Morrow, J. R. 2008. Mississippian
534 $\delta^{13}C_{carb}$ and conodont apatite $\delta^{18}O$ records – their relation to the Late Palaeozoic
535 glaciation. *Palaeogeography, Palaeoclimatology, Palaeoecology*, **268**, 273-292.

536 Cahyarini, S. Y, Pfeiffer, M., Timm, O., Dullo, W.-C. & Schönberg, D. G. 2008.
537 Reconstructing seawater $\delta^{18}O$ from paired coral $\delta^{18}O$ and Sr/Ca ratios: Methods, error
538 analysis and problems, with examples from Tahiti (French Polynesia) and Timor
539 (Indonesia). *Geochimica et Cosmochimica Acta*, **72**, 2841-2853.

540 Came, R.E., Eiler, J. M., Veizer, J., Zmy, K., Brand, U. & Weidman, C. R. 2007.
541 Coupling of surface temperatures and atmospheric CO_2 concentrations during the
542 Palaeozoic era. *Nature*, **449**, 198-201.

543 Cleal, C. J. & Thomas, B. A. 2005. Palaeozoic tropical rainforests and their effect on
544 global climates: is the past the key to the present? *Geobiology*, **3**, 13-31.

545 Compston, W. 1960. The carbon isotopic composition of certain marine invertebrates and
546 coals from the Australian Permian. *Geochimica et Cosmochimica Acta*, **18**, 1-22.

547 Conil R., Longestaey, P. J. & Ramsbottom, W. H. C. 1980. Matériaux pour l´étude
548 micropaléontologique du Dinantien de Grande-Bretagne. *Mémoires de l'Institut de*
549 Géologie de l´Université de Louvain **30**, 1–187 (imprinted 1979).

550 Conil, R., Groessens, E., Laloux, M., Poty, E. & Tourneur, F. 1991. Carboniferous guide
551 foraminifera, corals and conodonts in the Franco-Belgian and Campine basins. Their
552 potential for widespread correlation. *Courier Forschungsinstitut Senckenberg,* **130**, 15–
553 30.

554 Cózar, P. & Somerville I. D. 2004. New algal and foraminiferal assemblages and
555 evidence for recognition of the Asbian–Brigantian boundary in northern England.
556 *Proceedings of the Yorkshire Geological Society*, **55**, 43–65.

557 Cózar, P., Somerville, I. D. & Burgess, I. 2008. New foraminifers in the
558 Visean/Serpukhovian boundary interval of the Lower Limestone Formation, Midland
559 Valley, Scotland. *Journal of Paleontology*, **85**, 906-923.

560 Deconto, R. & Pollard, D. 2003. A coupled climate-ice sheet modelling approach to the
561 Early Cenozoic history of the Antarctic ice sheet. *Palaeogeography, Palaeoclimatology,*
562 *Palaeoecology*, **198**, 39-52.

563 Einor, O. L (Ed.). with Brazhnikova, N. E, Vassilyuk, N. P., Gorak, S. V., Dunaeva, N.
564 N., Kireeva, G. D., Kotchetkova, N. M., Popov, A. B., Potievskaya, P. D., Reitlinger, E.
565 A., Rotai, A. P., Sergeeva, M. T., Teteryuk, V. K., Fissunenko, O. P. & Furduy, R. S.
566 1979. The Lower-Middle Carboniferous Boundary. *In*: Wagner, R.H., Higgins, A.C.,
567 Meyen, S.V. (Eds.) *The Carboniferous of the USSR*, Yorkshire Geological Society,
568 Occasional Publication **4**. pp. 61–80.

569 Einor, O. L. 1996. The Former USSR. *In*: Wagner, R. H., Winkler Prins, C. F. &
570 Granados, L. F.(eds.) *The Carboniferous of the World III*, The Former USSR, Mongolia,
571 Middle Eastern Platform, Afghanistan and Iran. IUGS Publication 33. Instituto
572 Tecnológico Geominero de España- Nationaal Natuurhistorisch Museum. Madrid. pp. 3–
573 408.

574 England, J., Cusack, M., Paterson, N.W., Edwards, P., Lee, M.R. & Martin, R. 2006.
575 Hyperspectral cathodoluminescence imaging of modern and fossil carbonate shells.
576 *Journal of Geophysical Research,* **111**, G03001, doi:10.1029/2005JG000144.

577 Fewtrell, M. D., Ramsbottom W. H. C., Strank, A. R. E. 1981. Carboniferous. *In*: Jenkins
578 D. G. & Murray, J. W. (eds.) *Stratigraphical Atlas of fossil foraminifera* British
579 Micropalaeontological Society Series, Ellis Horwood. Chichester. pp. 15–69.

580 Fielding, C. R., Frank, T. D., Birgenheier, L. P., Rygel, M. C., Jones, A. T. & Roberts, J.
581 2008a. Stratigraphic imprint of the Late Palaeozoic Ice Age in eastern Australia: a record
582 of alternating glacial and nonglacial climate regime. *Journal of the Geological Society,*
583 *London*, **165**, 129-140.

584 Fielding, C. R., Frank, T. D. & Isbell, J. L 2008b. The late Paleozoic ice age – a review of
585 current understanding and synthesis of global climate patterns. *In*: Fielding, C. R., Frank,
586 T. D., and Isbell, J. L. (eds.) *Resolving the Late Paleozoic Ice Age in Time and Space*,
587 Geological Society of America Special Paper **441**, 343-354.

588 Frank, T. D., Birgenheier, L. P., Montanez, I. P., Fielding, C. R. & Rygel, M. C. 2008.
589 Late Paleozoic climate dynamics revealed by comparison of ice proximal stratigraphic
590 and ice-distal isotopic records. *In*: Fielding, C. R., Frank, T. D., and Isbell, J. L. (eds.)
591 *Resolving the Late Paleozoic Ice Age in Time and Space*, Geological Society of America
592 Special Paper **441**, 331-342.

593 Fraser, A. J. & Gawthorpe, R. L. 2003. *An atlas of Carboniferous basin evolution in*
594 *Northern England*. Geological Society, London, Memoir **28**.

595 Gibshman, N. B. 2001. Foraminiferal biostratigraphy of the Serpukhovian Stage
596 stratotype (Zaborie Quarry, Moscow Basin). *Newsletter on Carboniferous Stratigraphy*,
597 **19**, 31–34.

598 González-Bonorino, G. & Eyles, N. 1995. Inverse relation between ice extent and the late
599 Paleozoic glacial record of Gondwana. *Geology*, **23**, 1015-1018.

600 Gradstein, F. M., Ogg, J. G., Smith, A. G., Agterberg, F. P., Bleeker, W., Cooper, R. A.,
601 Davydov, V., Gibbard, P., Hinnov, L. A., House, M. R., Lourens, L., Luterbacher, H. P.,
602 McArthur, J., Melchin, M. J., Robb, L. J., Shergold, J., Villeneuve, M., Wardlaw, B. R.,
603 Ali, J., Brinkhuis, H., Hilgen, F. J., Hooker, J., Howarth, R. J., Knoll, A. H., Laskar, J.,
604 Monechi, S., Plumb, K. A., Powell, J., Raffi , I., Röhl, U., Sadler, P., Sanfi lippo, A.,
605 Schmitz, B., Shackleton, N. J., Shields, G. A., Strauss, H., Van Dam, J., van
606 Kolfschoten, T., Veizer, J. & Wilson, D., 2004, *A Geologic Time Scale* 2004: Cambridge,
607 Cambridge University Press, 589 p.

608 Griesshaber, E., Schmal, W. W., Neuser, R., Pettke, T., Blüm, M., Mutterlose, J & Brand,
609 U. 2007. Crystallographic texture and microstructure of terebratulide brachiopod shell
610 calcite: An optimized materials design with hierarchical architecture. *American*
611 *Mineralogist*, **92**, 722-734.

612 Grossman, E. L., Zhang, C. & Yancey, T. E. 1991. Stable isotope stratigraphy of
613 brachiopods from Pennsylvanian shales in Texas. *Geological Society of America Bulletin*,
614 **103**, 953-965.

615 Grossman, E. L., Mii, H. S. & Yancey, T. E. 1993. Stable isotopes in late Pennsylvanian
616 brachiopods from the United States: implications for Carboniferous paleoceanography.
617 *Geological Society of America Bulletin*, **105**, 1284-1296.

618 Grossman, E. L., Bruckschen, P., Mii, H-S., Chuvashov, B. I., Yancey, T. E. & Veizer, J
619 2002. Carboniferous paleoclimate and global change: isotopic evidence from the Russian
620 Platform. *In: Carboniferous Stratigraphy and Paleogeography in Eurasia*. Institute of
621 Geology and Geochemistry, Russian Academy of Sciences, Urals Branch, Ekaterinburg,
622 61-71.

623 Grossman, E. L., Yancey, T. E., Jones, T., Bruckschen, P., Chuvashov, B., Mazzullo, S.
624 & Mii, H-S., 2008. Glaciation, aridification, and carbon sequestration in the Permo-
625 Carboniferous: the isotopic record from low latitudes. *Palaeogeography,*
626 *Palaeoclimatology, Palaeoecology*, **269**, 1-16.

627 Heckel, P. H. & Clayton, G., 2006, The Carboniferous System: Use of the new official
628 names for the subsystems, series and stages: *Geologica Acta*, **4**, 403–407.

629 Immenhauser, A., Kenter, J. A. M., Ganssen, G., Bahamonde, J. R., Van Vliet, A. &
630 Saher, M. H. 2002. Origin and significance of isotope shifts in Pennsylvanian carbonates
631 (Asturias, NW Spain). *Journal of Sedimentary Research*, **72**, 82-94.

632 Isbell, J. L., Miller, M. F., Wolfe, K. L. & Lenaker, P. A. 2003. Timing of late Paleozoic
633 glaciation in Gondwana: was glaciation responsible for the development of northern
634 hemisphere cyclothems? *Geological Society of America Special Paper*, **370**, 5-24.

635 Joachimiski, M. M., Simon, L., van Geldern, R. & Lécuyer, C. 2005. Boron isotope
636 geochemistry of Paeozoic brachiopod calcite: Implications for a secular change on the

637 boron isotope geochemistry of seawater over the Phanerozoic. *Geochimica et*
638 *Cosmochimica Acta*, **69**, 4035-4044.

639 Johnson, G. A. L. 1984. Subsidence and sedimentation in the Northumberland Trough.
640 *Proceedings of the Yorkshire Geological Society*, **45**, 71-83.

641 Kim, S. T. & O'Neil, J. R. 1997. Equilibrium and non-equilibrium oxygen isotope effects
642 in synthetic carbonates. *Geochimica Cosmochimica Acta*, **61**, 3461-3475.

643 Korte, C., Kozur, H. W., Bruckschen, P. & Veizer, J. 2003. Strontium isotope evolution
644 of Late Permian and Triassic seawater. *Geochimica Cosmochimica Acta,* **67**, 47-62.

645 Korte, C., Jasper, T., Kozur, H. W. & Veizer, J. 2005. $\delta^{18}O$ and $\delta^{13}C$ of Permian
646 brachiopods: A record of seawater evolution and continental glaciation.
647 *Palaeogeography, Palaeoclimatology, Palaeoecology,* **224**, 333-351.

648 Leng, M. J. & Marshall, J. D. 2004. Palaeoclimate interpretation of stable isotope data
649 from lake sediments. *Quaternary Science Reviews*, **23**, 811-831.

650 McArthur, J. M., Crame, J. A. & Thirlwall, M. F. 2000. Definition of Late Cretaceous
651 stage boundaries in Antarctica using strontium isotope stratigraphy. *Journal of Geology*,
652 **108**, 623-640.

653 Menning, M., Weyer, D., Drozdzewski, G., van Amerom, H. W. J. & Wendt, I. 2000. A
654 Carboniferous time scale 2000: Discussion and use of geological parameters as time
655 indicators from Central and Western Europe. *Geologisches Jahrbuch*, **A156**, 3–44.

656 Mii, H.-S., Grossman, E.L., and Yancey, T.E., 1999, Carboniferous isotope stratigraphies
657 of North America; implications for Carboniferous paleoceanography and Mississippian

glaciation: *Geological Society of America Bulletin*, **111**, 960–973, doi: 10.1130/0016-7606(1999)111 <0960:CISONA>2.3.CO; 2.

Mii, H.-S., Grossman, E.L., Yancey, T.E., Chuvashov, B. & Egorov, A. 2001. Isotopic records of brachiopod shells from the Russian Platform – evidence for the onset of Mid-Carboniferous glaciation. *Chemical Geology*, **175**, 133-147.

Mills, D. A. C. & Hull, J. H. 1968. The geological survey borehole at Woodland, Co. Durham. *Bulletin of the Geological Survey of Great Britain* No. **28**, 1-38.

Neves, R. 1968. The palynology of the Woodland Borehole, Co. Durham. *Bulletin of the Geological Survey of Great Britain* No. **28**, 55-60.

Owens, B., McLean, D. & Bodman, D. 2004. A revised palynozonation of British Namurian deposits and comparisons with eastern Europe. *Micropaleontology*, **50**, 89-103.

Parkinson, D., Curry, G. B., Cusack, M. & Fallick, A. E. 2005. Shell structure, patterns and trends of oxygen and carbon stable isotopes in modern brachiopod shells. *Chemical Geology*, **219**, 193-235.

Pearson, P. N. & Palmer, M. R. 2000. Atmospheric carbon dioxide over the past 60 million years. *Nature*, **406**, 695-699.

Peters-Kottig, W. Strauss, H. & Kerp, H. 2006. The land plant $\delta^{13}C$ record and plant evolution in the Late Palaeozoic. *Palaeogeography, Palaeoclimatology, Palaeoecology*, **240**, 237-252.

Popp, B. N., Anderson, T. F. & Sandberg, P. A. 1986. Brachiopods as indicators of original isotopic compositions in some Paleozoic limestones. *Geological Society of America Bulletin*, **97**, 1262-1269.

680 Riley, N. J. R. 1992. Foraminiferal and algal biostratigraphy of Rowlands Gill Borehole,
681 (BGS BH reference NZ15NE/276). *Report of the Palaeontological Department, British*
682 *Geological Survey*, Report **PDL 92/132R**.

683 Samtlemben, C., Munnecke, A., Bickert, T. & Pätzold, J. 2001. Shell succession,
684 assemblage and species dependent effects on C/O-isotopic composition of brachiopods –
685 examples from the Silurian of Gotland. *Chemical Geology*, **175,** 61-107.

686 Stephenson, M. H., Leng, M. J., Vane, C. H., Osterloff, P. L. & Arrowsmith C. 2005.
687 Investigating the record of Permian climate change from argillaceous sediments, Oman.
688 *Journal of the Geological Society, London*, **162**, 641-651.

689 Stephenson, M. H., Millward, D., Leng M. J. & Vane C. H. 2008. Palaeoecological and
690 possible evolutionary effects of early Namurian (Serpukhovian, Carboniferous)
691 glacioeustatic cyclicity. *Journal of the Geological Society*, **165**, 993-1005

692 Steuber T. & Veizer J. 2003. Phanerozoic record of plate tectonic control of seawater
693 chemistry and carbonate sedimentation. *Geology*, **30,** 1123–1126.

694 Strauss, H. & Peters-Kottig, W. 2003. The Paleozoic to Mesozoic carbon cycle revisited:
695 the carbon isotopic composition of terrestrial organic matter. *Geochemistry, Geophysics,*
696 *Geosystems*, **4**, Article Number 10, 1-15.

697 Tucker, M. E., Gallagher, J., & Leng, M. J. 2009. Are beds in shelf carbonates millennial-
698 scale cycles? An example from the mid-Carboniferous of northern England. *Sedimentary*
699 *Geology*, **214**, 19-34.

Van Geldern R., Joachimski M. M., Day J., Jansen U., Alvarez F., Yolkin E. A. & Ma X.-P. 2006. Carbon, oxygen and strontium isotope records of Devonian brachiopod shell calcite. *Palaeoegeography, Palaeoclimatology, Palaeoecology*, **240**, 47-67.

Vdovenko, M. V. 2001. Atlas of foraminifera from the Upper Viséan and Lower Serpukhovian (Lower Carboniferous) of the Donets Basin (Ukraine). *Abhandlungen und Berichte für Naturkunde,* **23**, 93–178.

Veizer, J., Ala, D., Azmy, K., Bruckschen, P., Buhl, D., Bruhn, F., Carden, G.A.F., Diener, A., Ebneth, S., Godderis, Y., Jasper, T., Korte, C., Pawellek, F., Podlaha, O.G. & Strass, H. 1999. $^{87}Sr/^{86}Sr$, $\delta^{18}O$ and $\delta^{13}C$ evolution of Phanerozoic seawater. *Chemical Geology*, **161**, 59-88.

Williams, A., Brunton, H., Carlson, S. J. *et al.* (45 authors) 2007. *Treatise on invertebrate palaeontology (part H, Brachiopoda revised). Volume 6: Supplement*. Geological Society of America, Boulder, and University of Kansas Press, Lawrence.

Figure captions

Fig. 1. Correlation of late Visean and Namurian stages, substages and biozones after Cózar *et al.* 2008 and Owens *et al.* (2004). Radiometric dates from Gradstein *et al.* (2004).

Fig. 2a. Block and basin distribution in the Namurian, simplified after Fraser & Gawthorpe (2003). Location of the Woodland, Throckley and Rowlands Gill boreholes shown in Figure 2b.

720 Fig. 3. Brachiopod $\delta^{18}O$ and $\delta^{13}C$ in the Woodland Borehole. Figures show the number of
721 analyses from single horizons from which multiple brachiopods were sampled.

722 Fig. 4. Correlation of the Woodland, Throckley and Rowlands Gill boreholes showing
723 $\delta^{13}C_{org}$ data from the Throckley and Rowlands Gill boreholes. Key to lithologies as in
724 Figure 3. Data from Throckley and Rowlands Gill boreholes from Stephenson *et al.*
725 (2008).

726 Fig. 5. Foraminifera from the Woodland Borehole. (**a**) *Monotaxinoides priscus*, BLA646,
727 Four Fathom Lst. (**b**) *Monotaxinoides subconica*, BLA91, Great Lst. (**c**) *Monotaxinoides*
728 *subplana*, BLA578, Four Fathom Lst. (**d**) *Monotaxinoides transitorius*, BU6179,
729 Whitehouse Lst. (**e**) *Archaediscus longus*, BU9078, Crag Lst. (**f**) *Archaediscus*
730 *postmoelleri*, BU9437, Shelly Lst. (**g**) *Archaediscus* cf. *brazhnikovae*, BU9078, Crag Lst.
731 (**h**) *Tubispirodiscus hosiensis*, BLA23, Great Lst. (**i**) *Asteroarchaediscus bashkiricus*,
732 BU8301, Rookhope Shell-Beds Limestone. (**j**) *Archaediscus donetzianus*, BU8815, Crag
733 Lst. (**k**) *Eosigmoilina robertsoni*, BU8277, Rookhope Shell-Beds Limestone. (**l**)
734 *Neoarchaediscus postrugosus*, BLA91, Great Lst. (**m**) *Eostaffella acutiformis*, BLA211,
735 Great Lst. (**n**) *Eostaffella postmosquensis*, BU8326, Rookhope Shell-Beds Limestone. (**o**)
736 *Eostaffella angusta*, BLA181, Great Lst. (**p**) *Eostaffella chusovensis*, BLA211, Great Lst.
737 (**q**) *Eostaffellina paraprotvae*, BU7353, Grindstone Lst. (**r**) *Eostaffellina protvae*,
738 BU8326, Rookhope Shell-Beds Limestone. (**s**) *Eostaffella paraumbilicata*, BU8326,
739 Rookhope Shell-Beds Limestone. (**t**) *Eostaffella chomatifera*, BLA91, Great Lst. (**u**)
740 *Plectostaffella bogdanovensis*, BU6179. Whitehouse Lst. (**v**) *Seminovella*? *kazashtanika*
741 BU6179. Whitehouse Lst. (**w**) *Seminovella* cf. *elegantula*, oblique section, BU6179.
742 Whitehouse Lst. (**x**) *Seminovella elegantula*, BU7353, Grindstone Lst. (**y**) *Plectostaffella*

varvariensis, BU8277, Rookhope Shell-Beds Limestone. (**z**) *Plectostaffella jahkensis*, BU8326, Rookhope Shell-Bed Limestone.

Fig. 6. Ultrastructure of brachiopod shells from the Woodland Borehole. (**a**) Well-preserved secondary layer fibres with keel and saddle outline (BU8212), scale bar 20 µm. (**b**) Longitudinal profile of well-preserved secondary layer fibres (BU8236), scale bar 10 µm. (**c**) Well-preserved secondary layer fibres with keel and saddle outline (BU8240), scale bar 5 µm. (**d**) Well-preserved tertiary layers (BU8212), scale bar 200 µm. (**e**)-(**h**) Well preserved tertiary layer with discrete prisms and growth banding (BU8285), scale bars 100 µm (e), 50 µm (f), 100 µm (g), 20 µm (h). (**i**) Well-preserved tertiary layer with detail of the growth bands (BU8389), scale bar 50 µm. (**j**) Secondary and tertiary layers affected by bio-erosion (BU9142), scale bar 200 µm. (**k**) Diagenetically altered secondary layer fibres (BU7624) corresponding to type-3 ultrastructure of Samtleben *et al.* (2001), scale bar 50 µm. (**l**) Altered secondary layer corresponding to type-6 ultrastructure of Samtleben *et al.* (2001), (BU9197), scale bar 20 µm. (**m**), (**n**) well preserved alternation of secondary and tertiary layer, (BU6768), scale bars 200 µm and 500 µm. (**o**) Diagenetically altered laminar secondary layer (BU8576), corresponding to type-9 ultrastructure of Samtleben *et al.* (2001), scale bar 50 µm.

Fig. 7. Woodland Borehole brachiopod cathodoluminescence. (**a**), (**b**) Non-luminescent well preserved shell (sample 19, BU8240 *Skelidorigma* sp.), scale bar 1 mm. (**c**) Preserved shell layered structure *of Angiospirifer* sp. (sample 12, BU7624) with internal cloudy prismatic calcitic cement, scale bar 1 mm. (**d**)-(**e**)-(**f**) Non-luminescent prismatic tertiary layer coated by a thin isophacous red bright luminescent cement (dog tooth calcite) (Sample 23, BU8285. *Anthracospirifer* sp.). Scale bar 1 mm. (**g**)-(**h**)-(**i**) Non

luminescent tertiary layer (sample 21, BU8285 *Anthracospirifer* sp.) in a bright luminescent shaly bioclastic matrix. Scale bar 2 mm. (**j**), (**k**) Luminescent/non luminescent secondary layer (sample 3, BU6768 *Antiquatonia hindi*) Scale bar 2 mm. (**l**) Partially luminescent shell (sample 6, BU6782 *Productus carbonarius*). Scale bar 1 mm. (**m**), (**n**) Non luminescent secondary and tertiary layers (sample 34, BU8576 *Antiquatonia costata* with luminescent cement. Scale bar 1 mm. (**o**) Luminescent secondary layer with pseudopuncta (sample 11, BU7587 Dyctioclostinae). Scale bar 2 mm.

<table>
<tr><th>European stages</th><th>British substages</th><th>Goniatite biozones</th><th>Paly biozones</th><th>Horizons/ subst. in the Moscow Basin</th><th>International stages</th><th>Range of O,C
This study (brachs)</th><th>Range of $d^{13}C_{org}$
This study</th><th>Glacial Periods
Isbell et al. 2003</th><th>Glacial Periods
E. Australia, Fielding et al. 2008a</th></tr>
<tr><td rowspan="2">Late Namurian</td><td rowspan="2">Chokierian</td><td rowspan="2">H1</td><td rowspan="2">SO</td><td rowspan="2">No deposition</td><td rowspan="2">Early Bashkirian
318.1 +/-1.3</td><td rowspan="3"></td><td rowspan="4"></td><td rowspan="5">Glacial II</td><td rowspan="2">?</td></tr>
<tr><td rowspan="3">C2</td></tr>
<tr><td rowspan="3">Early Namurian</td><td rowspan="2">Arnsbergian</td><td rowspan="2">E2</td><td rowspan="2">TK</td><td>Pestovskian</td><td rowspan="3">Serpukhovian
326.4 +/-1.6</td></tr>
<tr><td>Protvinskian</td><td rowspan="2">?</td></tr>
<tr><td rowspan="2">Pendleian</td><td rowspan="2">E1</td><td rowspan="3">CN</td><td>Steshevskian</td><td rowspan="2"></td><td rowspan="2">?</td></tr>
<tr><td>Tarouskian</td><td rowspan="2"></td><td rowspan="2">C1</td></tr>
<tr><td>Late Visean</td><td>Late Brigantian</td><td>P2</td><td></td><td>Late Visean</td><td></td><td></td><td>?</td></tr>
</table>

Fig 1

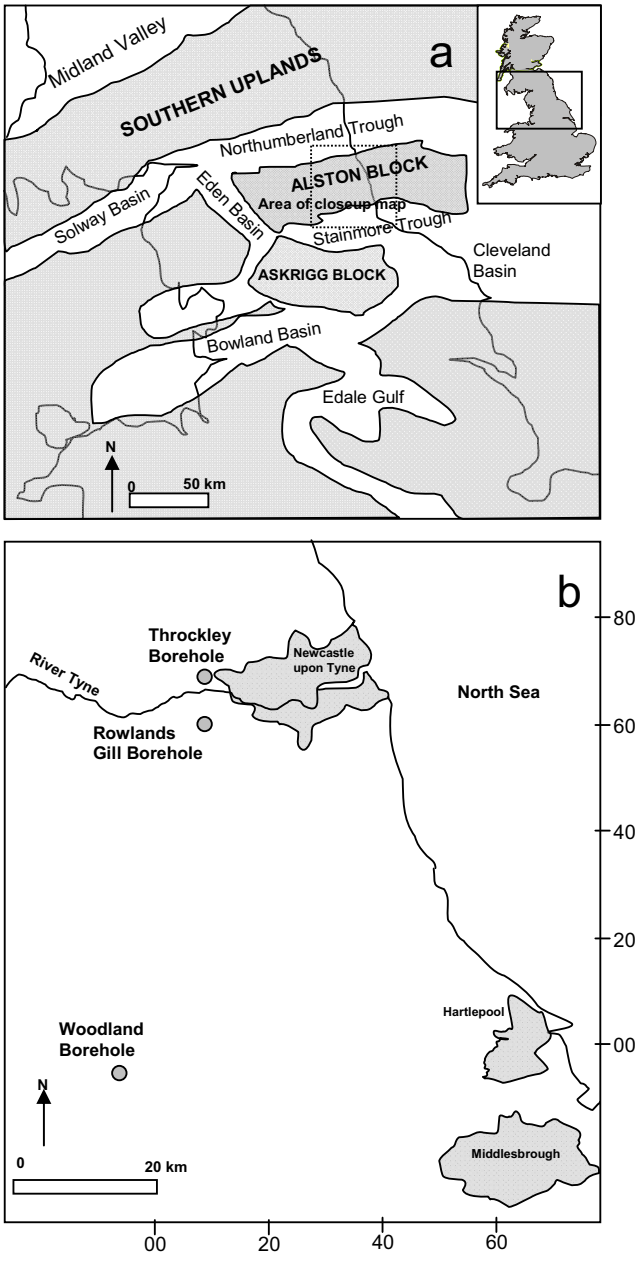
a
Midland Valley
SOUTHERN UPLANDS
Northumberland Trough
ALSTON BLOCK
Area of closeup map
Solway Basin
Eden Basin
Stainmore Trough
Cleveland Basin
ASKRIGG BLOCK
Bowland Basin
Edale Gulf
N
0
50 km
b
Throckley Borehole
Newcastle upon Tyne
River Tyne
North Sea
Rowlands Gill Borehole
Hartlepool
Woodland Borehole
Middlesbrough
N
0
20 km
80
60
40
20
00
00
20
40
60

Fig 2

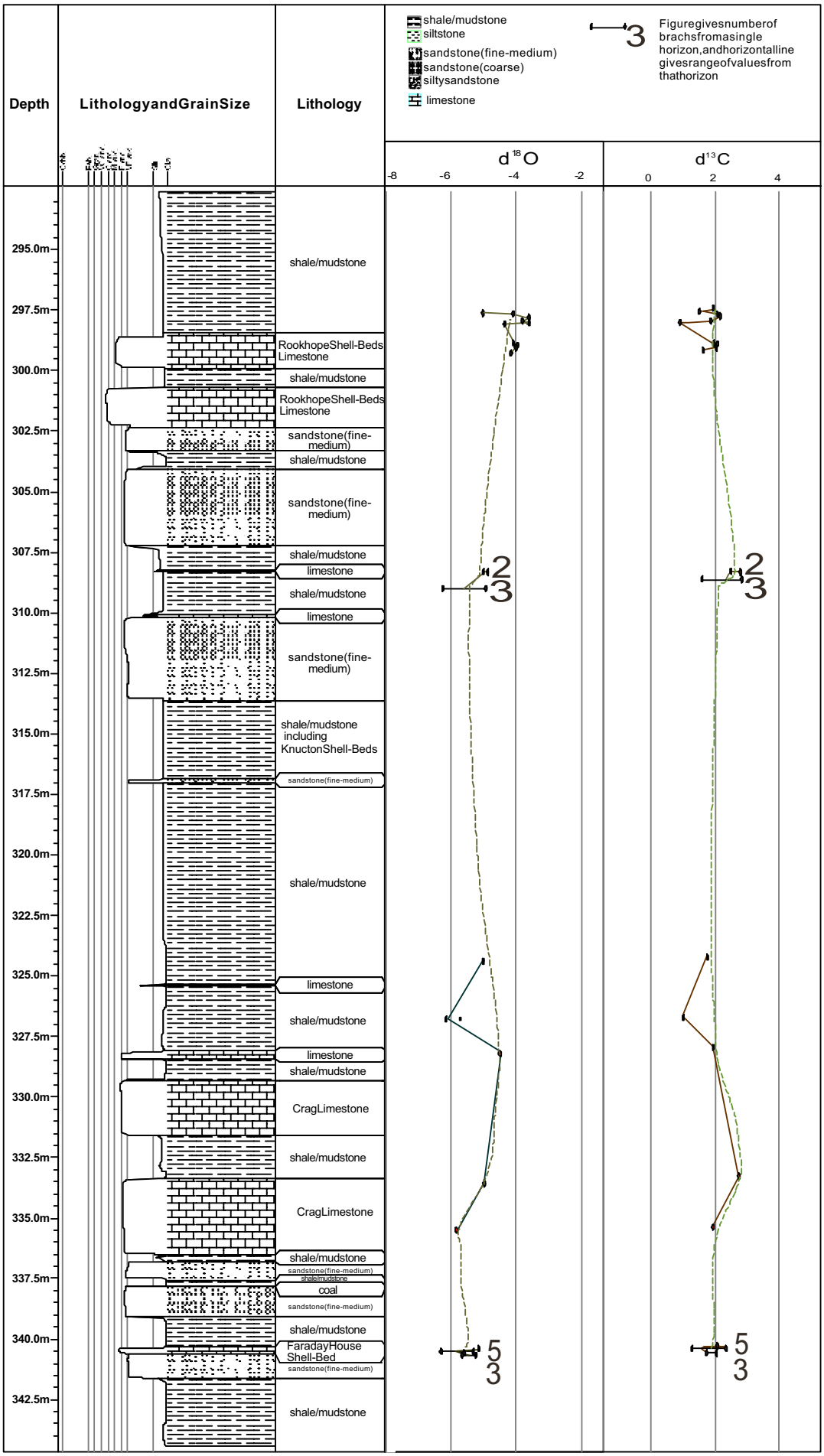
Depth
LithologyandGrainSize
Lithology
shale/mudstone
siltstone
sandstone(fine-medium)
sandstone(coarse)
siltysandstone
limestone
3
Figuregivesnumberof brachsfromasingle horizon,andhorizontalline givesrangeofvaluesfrom thathorizon
d18O
-8
-6
-4
-2
d13C
0
2
4
295.0m
297.5m
300.0m
302.5m
305.0m
307.5m
310.0m
312.5m
315.0m
317.5m
320.0m
322.5m
325.0m
327.5m
330.0m
332.5m
335.0m
337.5m
340.0m
342.5m
shale/mudstone
RookhopeShell-Beds Limestone
shale/mudstone
RookhopeShell-Beds Limestone
sandstone(fine-medium)
shale/mudstone
sandstone(fine-medium)
shale/mudstone
limestone
shale/mudstone
limestone
sandstone(fine-medium)
shale/mudstone including KnuctonShell-Beds
sandstone(fine-medium)
shale/mudstone
limestone
shale/mudstone
limestone
shale/mudstone
CragLimestone
shale/mudstone
CragLimestone
shale/mudstone
sandstone(fine-medium)
shale/mudstone
coal
sandstone(fine-medium)
shale/mudstone
FaradayHouse Shell-Bed
sandstone(fine-medium)
shale/mudstone
2
3
2
3
5
3
5
3

Fig 3

Fig 4

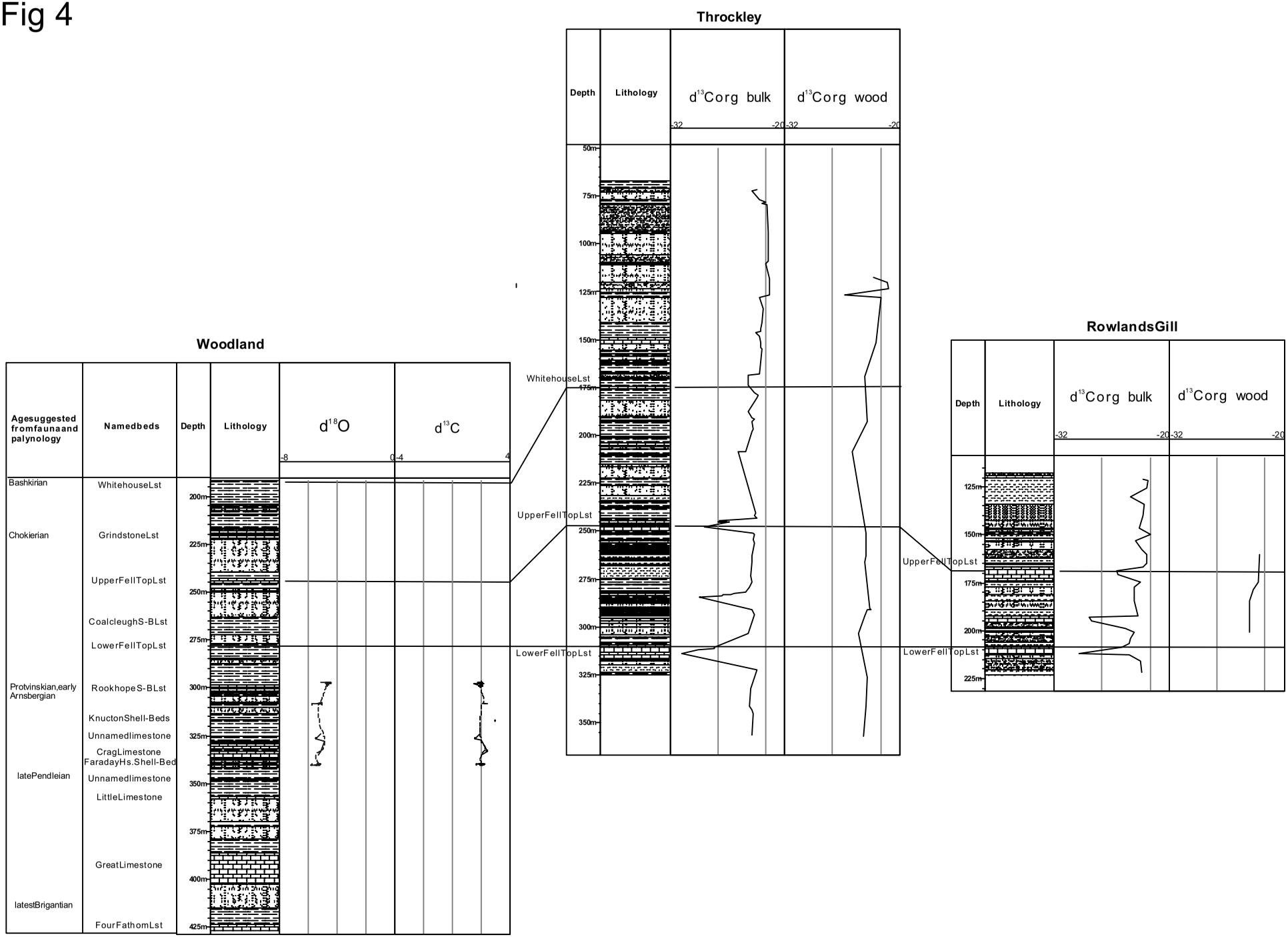
Throckley
Depth
Lithology
d13Corg bulk
d13Corg wood
-32
-20
50m
75m
100m
125m
150m
175m
200m
225m
250m
275m
300m
325m
350m
Woodland
Agesuggested fromfaunaand palynology
Namedbeds
Depth
Lithology
d18O
d13C
-8
0
4
Bashkirian
Chokierian
Protvinskian,early Arnsbergian
latePendleian
latestBrigantian
WhitehouseLst
GrindstoneLst
UpperFellTopLst
CoalcleughS-BLst
LowerFellTopLst
RookhopeS-BLst
KnuctonShell-Beds
Unnamedlimestone
CragLimestone
FaradayHs.Shell-Bed
Unnamedlimestone
LittleLimestone
GreatLimestone
FourFathomLst
200m
225m
250m
275m
300m
325m
350m
375m
400m
425m
WhitehouseLst
UpperFellTopLst
LowerFellTopLst
RowlandsGill
Depth
Lithology
d13Corg bulk
d13Corg wood
-32
-20
125m
150m
175m
200m
225m
UpperFellTopLst
LowerFellTopLst


a
b
c
d
e
f
g
h
i
j
k
l
m
n
o
p
q
r
s
t
u
v
w
x
y
z
200 microns

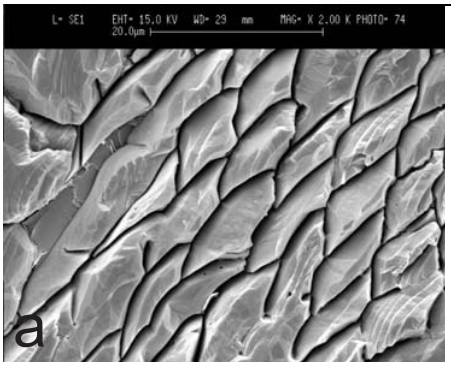
a

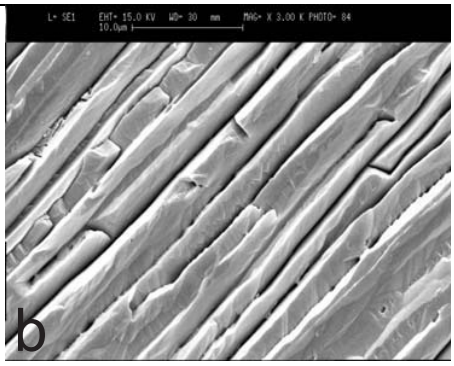
b

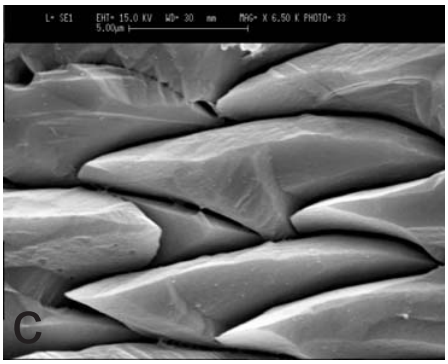
c

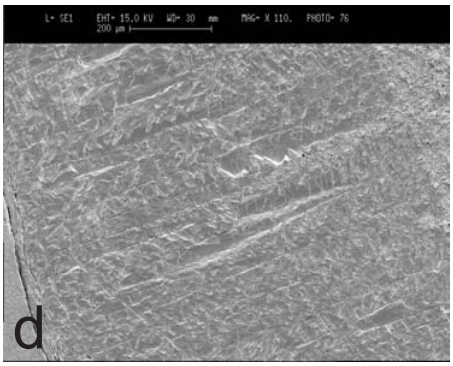
d

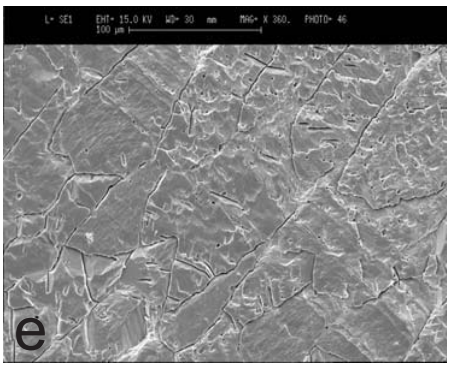
e

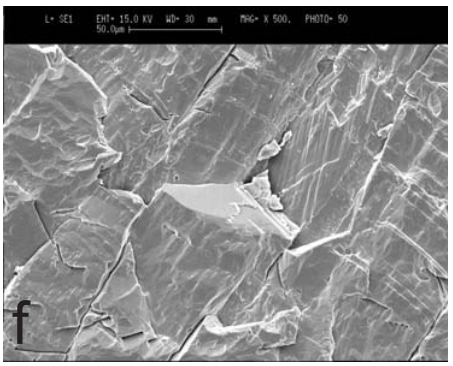
f

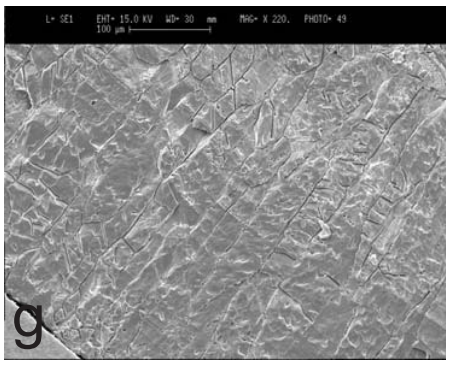
g

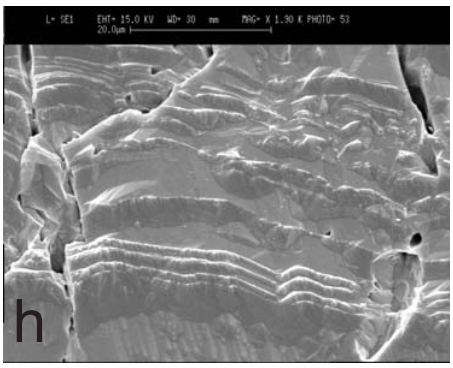
h

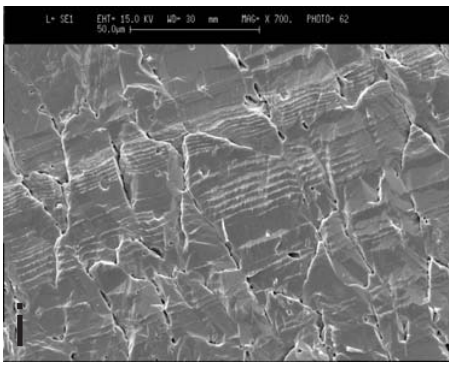
i

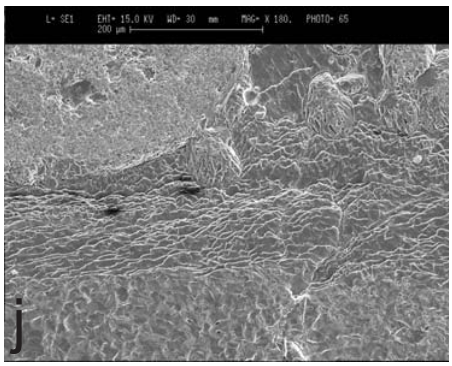
j

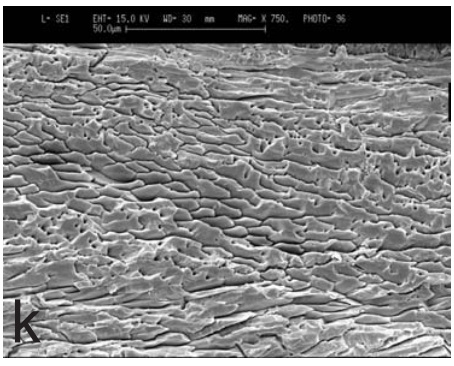
k

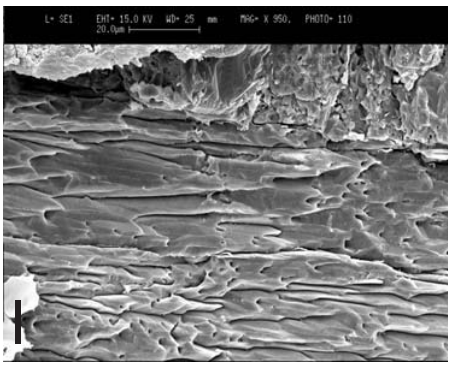
ł

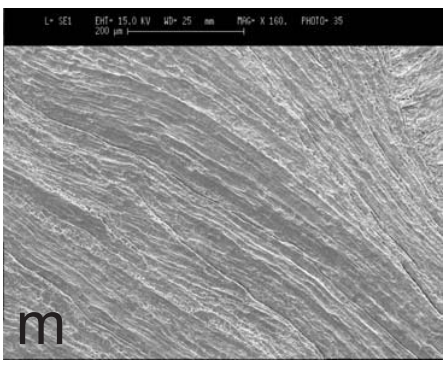
m

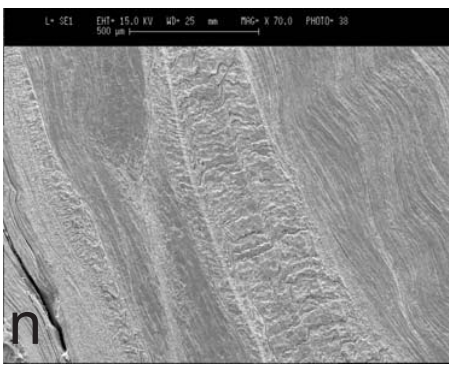
n

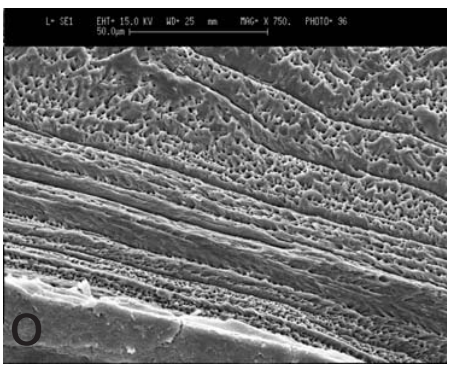
o

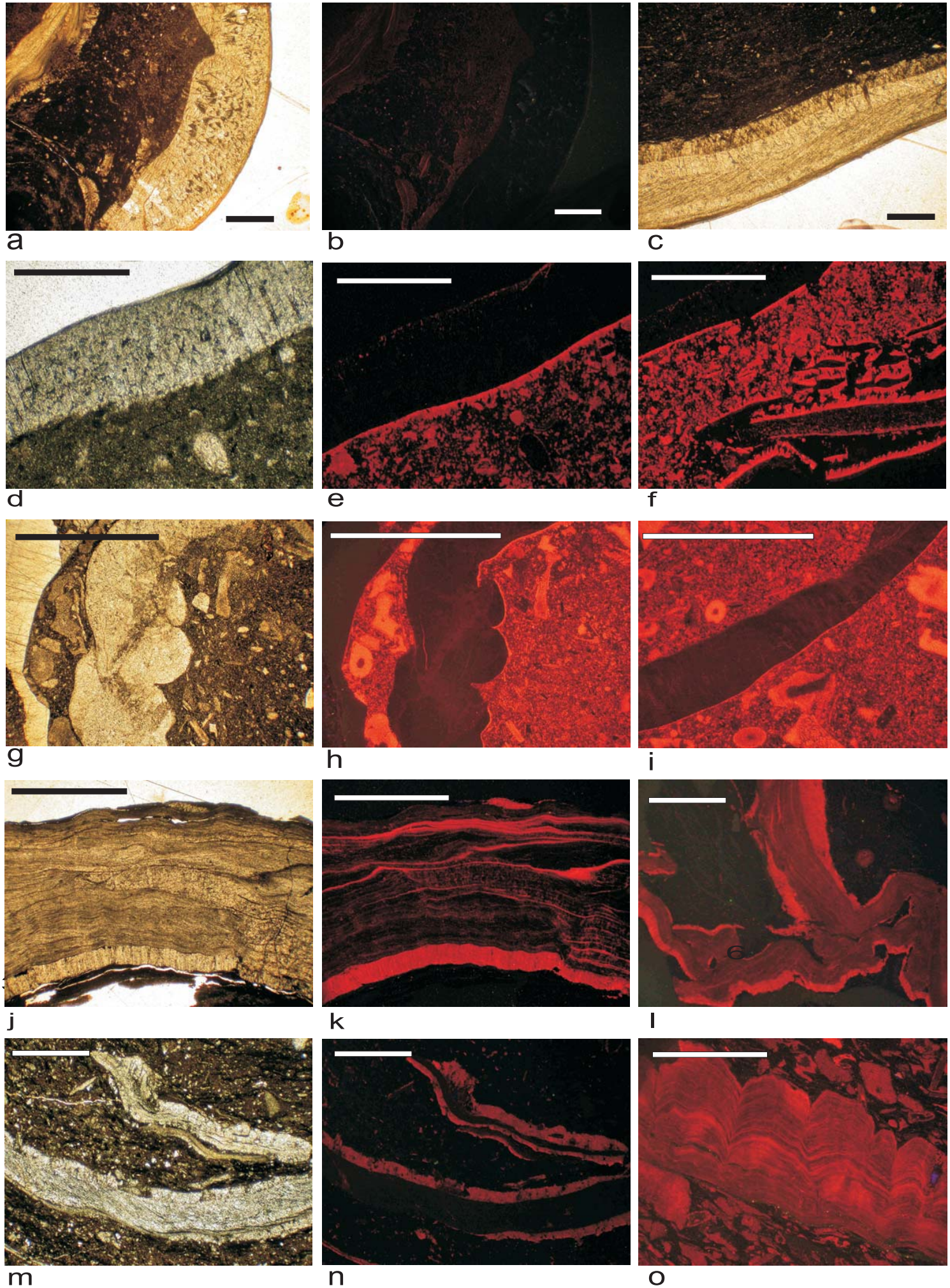
a
b
c
d
e
f
g
h
i
j
k
l
m
n
o

Number	Reg series	Reg No	Spec.	Taxon	Ultrastructure	Cathodoluminescence	Depth	d13C	d18O	Mg	Ba	Sr	Mn	Fe
1	BU	6578	A	Antiquatonia hindi	slightly altered	PL	193.09	+1.9	-5.8					
3	BU	6768	A	Antiquatonia hindi	well preserved	NL, PL, L	195.81	+0.8	-4.9					
4	BU	6778	V	Productus carbonarius	altered	PL	195.86	+1.8	-6.7					
5	BU	6779	V	Productus carbonarius	altered	L	195.86	-0.4	-11.6					
6	BU	6782	V	Productus carbonarius	altered	PL	195.86	+0.4	-7.3					
7	BU	6789	V	Productus carbonarius	altered	L	195.94	-0.0	-10.7					
9	BU	7370	V	Angiospirifer sp.	altered	NL	219.59	+2.4	-5.7					
10	BU	7422	V	Spiriferid	slightly altered	PL	220.07	-0.9	-6.7					
11	BU	7587	V	Dictyoclostinae	slightly altered	L	243.56	+0.4	-8.1					
12	BU	7624	V	Angiospirifer sp.	well preserved	NL	244.07	+0.8	-5.3					
13	BU	8196	V	Skelidorygma sp.	II altered externally - III well preserve	NL	297.60	+1.5	-5.2	1764	<DL	835	97	2516
14	BU	8200	V	Skelidorygma sp.	II-III well preserved	PL	297.68	+2.1	-4.0	1201	<DL	718	79	1030
15	BU	8212	V	Skelidorygma sp.	II-III well preserved	NL	297.82	-2.0	-3.4					
16	BU	8221	V	Skelidorygma sp.	II-III well preserved	NL	297.91	+2.2	-3.6					
17	BU	8230	V	Skelidorygma sp.	II-III well preserved	NL	297.97	+1.8	-3.4					
18	BU	8236	V	Skelidorygma sp.	II-III well preserved	NL	298.05	+0.9	-4.3					
19	BU	8240	V	Skelidorygma sp.	II-III well preserved but fractures	PL	298.05	+0.6	-6.0					
21	BU	8282	V	Anthracospirifer sp.	III well preserved	NL	298.91	+2.0	-4.0	976	<DL	620	27	587
23	BU	8285	V	Anthracospirifer sp.	III well preserved	NL	298.75	+2.1	-3.7					
24	BU	8286	V	Anthracospirifer sp.	no data		299.09	+2.1	-3.8	985	<DL	554	50	709
25	BU	8292	A	Angiospirifer trigonalis	II-III well preserved	NL	299.29	+1.5	-4.1					
27	BU	8370	V	Anthracospirifer sp.	II-III well preserved	NL	308.32	+3.1	-5.0	825	<DL	535	85	1169
28	BU	8379	V	Anthracospirifer sp.	no data	NL	308.32	+2.7	-5.2	994	<DL	616	207	2732
29	BU	8389	V	Anthracospirifer sp.	III well preserved	NL	308.46							
30	BU	8415	V	Anthracospirifer sp.	altered	NL	308.84	+2.6	-6.3	620	<DL	762	64	1362
31	BU	8419	V	Anthracospirifer sp.	II-III well preserved	NL	308.97	+1.6	-6.9	1171	<DL	898	203	1533
32	BU	8421	A	Anthracospirifer sp.	II-III well preserved	NL	308.97	+3.2	-5.1	813	<DL	535	21	167
32bis	BU	8421	V	Anthracospirifer sp.	II-III well preserved	NL	308.97	+2.1	-5.1	689	<DL	732	48	649
33	BU	8572	D	Anthracospirifer sp.	II-III well preserved	NL- Lrim	324.23	+1.7	-5.2	1248	<DL	939	104	2641
34	BU	8576	V	Antiquatonia costata	II altered	NL- Lrim	324.03	+0.6	-8.5					
35	BU	8654	V	Anthracospirifer sp.	II altered - III preserved	PL	325.49	+1.3	-7.2					
36	BU	8695	V	Anthracospirifer sp.	III well preserved	NL- Lrim	326.75	+0.7	-6.1	6487	<DL	<DL	<DL	<DL
37	BU	8775	V	Anthracospirifer sp.	II-III well preserved	NL	328.16	+1.9	-4.5					
38	BU	8950	D	Merospirifer sp.	altered		331.98	+2.2	-7.3	1740	37	1127	68	5654
39	BU	9004	V	Anthracospirifer sp.	II-III well preserved	NL	333.56	+3.1	-5.2					
40	BU	9055	V	Anthracospirifer sp.	III well preserved	NL	335.50	+1.9	-5.7					
41	BU	9129	V	Anthracospirifer sp.	II-III well preserved	NL	340.38	+2.1	-5.4	501	<DL	758	36	1163
42	BU	9142	V	Angiospirifer sp.	II-III well preserved	NL	340.45	+2.3	-6.0	1270	14	925	144	4072
42bis	BU	9142	D	Angiospirifer sp.	II-III with bioerosion	NL	340.45	+1.6	-6.9					
43	BU	9143	V	Angiospirifer sp.	II-III well preserved	NL	340.45	+2.5	-6.2	611	7	916	70	906
44	BU	9147	V	Angiospirifer sp.	II-III well preserved	NL	340.45	+1.6	-6.3	420	7	803	27	705
45	BU	9149	V	Anthracospirifer sp.	III well preserved	NL	340.45	+1.5	-5.6					
46	BU	9154	V	Anthracospirifer sp.	II-III well preserved	NL	340.53	+1.4	-5.9					
47	BU	9157	V	Angiospirifer sp.	II-III well preserved	NL	340.62	+1.5	-5.9					
49A	BU	9161	V	Angiospirifer trigonalis	altered	PL	340.62	+1.7	-7.6					
49B	BU	9161	V	Angiospirifer trigonalis	III preserved	NL	340.62	+2.0	-6.0	279	11	764	18	241
50	BU	9162	V	Anthracospirifer sp.	II-III well preserved	NL	340.62	+2.1	-5.5	303	<DL	743	10	106
Calcareous mudstone associated with BU 8196							297.60			56204	585	1853	2796	236454
Calcareous mudstone associated with BU 8572							324.23			45040	449	2277	2159	496589

NL non luminescent, L luminescent; PL partally luminescent; Lrim luminsecent rim <DL less than detection limit; D Dorsal; V ventral